Taylor & Francis
Taylor & Francis Group

Atmospheric and Oceanic Science Letters

ISSN: (Print) (Online) Journal homepage: https://www.tandfonline.com/loi/taos20

Properties of summer radiation and aerosols at Xinzhou, a suburban site on the North China Plain

Jinqiang ZHANG , Jun ZHU & Xiang'ao XIA

To cite this article: Jinqiang ZHANG , Jun ZHU & Xiang'ao XIA (2020): Properties of summer radiation and aerosols at Xinzhou, a suburban site on the North China Plain, Atmospheric and Oceanic Science Letters, DOI: 10.1080/16742834.2020.1820302

To link to this article: https://doi.org/10.1080/16742834.2020.1820302

Published online: 20 Sep 2020.

ATMOSPHERIC AND OCEANIC SCIENCE LETTERS
https://doi.org/10.1080/16742834.2020.1820302

Taylor & Francis
Taylor & Francis Group

Properties of summer radiation and aerosols at Xinzhou, a suburban site on the North China Plain

ZHANG Jinqiang[a,b,c], ZHU Jun[b,d] and XIA Xiang'ao[a,b,c]

[a]Key Laboratory of Middle Atmosphere and Global Environment Observation, Institute of Atmospheric Physics, Chinese Academy of Sciences, Beijing, China; [b]Collaborative Innovation Center on Forecast and Evaluation of Meteorological Disasters, Nanjing University of Information Science & Technology, Nanjing, China; [c]College of Earth and Planetary Science, University of Chinese Academy of Sciences, Beijing, China; [d]Key Laboratory for Aerosol–Cloud–Precipitation of the China Meteorological Administration, Nanjing University of Information Science and Technology, Nanjing, China

ABSTRACT

The properties of summer radiation and aerosols were studied at Xinzhou, a suburban site on the North China Plain (NCP) by using ground-based measurements in 2014. The radiation detections under clear and cloudy skies showed that longwave radiation presented a sigmate pattern, with a maximum of 392.6 W m^{-2} at 1700 local standard time (LST) associated with the cloud radiative forcing, and a minimum of 360.0 W m^{-2} at 0600 LST when the lowest surface temperature (17.1°C) occurred. Solar radiation, including global, direct, diffuse, photosynthetically active, ultraviolet-A, and ultraviolet-B, exhibited a single peak at ~1300 LST. A bimodal size distribution, with fine mode aerosols showing a peak between 0.1 and 0.2 μm and coarse mode aerosols showing a peak at ~5 μm, was observed at Xinzhou. The dominant aerosol type was black carbon coating on coarse particles (85.7%) for the cases with aerosol optical depth at 400 nm (AOD) greater than 0.4, leading to a lower single scattering albedo (0.81) than the typical value (~0.90) at the other stations on the NCP. The mean values of EAE and AAE (extinction and absorption Ångström exponent, respectively) were 1.14 ± 0.15 and 0.58 ± 0.28 for the aerosol measurements. The average of instantaneous aerosol direct radiative forcing at the bottom of the atmosphere was −138.9 ± 33.0 W m^{-2} for the cases with AOD > 0.4. The results in this study are expected to improve understanding at suburban sites on the NCP of aerosol properties and their impacts on regional radiation budgets.

ARTICLE HISTORY
Received 17 January 2020
Revised 7 April 2020
Accepted 7 April 2020

KEYWORDS
Radiation; aerosols; suburban site; North China Plain

关键词
辐射; 气溶胶; 郊区站点; 华北平原

华北平原忻州郊区站点夏季辐射和气溶胶特性研究

摘要

基于2014年夏季地基观测数据分析了华北平原忻州郊区站点辐射和气溶胶特性。结果表明，晴空和云天条件下的长波辐射最大值和最小值分别出现在地方时17:00 (392.6 W m^{-2}) 和06:00 (360.0 W m^{-2})；总辐射，直接辐射，散射辐射，光合有效辐射，紫外A和紫外B辐射最大值出现在~13:00。气溶胶粒径呈双峰结构，粗细模态峰值分别为~5微米和0.1–0.2微米。气溶胶光学厚度大于0.4 (400 nm) 时主要为黑碳覆盖粗粒子类型气溶胶 (85.7%)，使得气溶胶单次散射反照率 (0.81) 低于华北平原其他测站典型值 (~0.90)；消光和吸收埃斯特朗指数平均值分别为1.14 ± 0.15和0.58 ± 0.28；地表气溶胶直接辐射强迫瞬时平均值为−138.9 ± 33.0 W m^{-2}。

1. Introduction

Radiation and aerosols can greatly affect climate change and human and terrestrial environments (Pounds 2001; Anderson et al. 2003; Garrett and Zhao 2006). Both parameters are highly variable on temporal and spatial scales (e.g., Yang et al. 2016a; Fan, Zhao, and Yang 2020). Many approaches have been proposed for estimating radiation budgets, such as the surface measurements from the Baseline Surface Radiation Network (BSRN) of the World Climate Research Program, available since 1992 (Ohmura et al. 1998). This global network provides surface radiative flux data at the highest possible accuracy since its instrumentation is well calibrated and deployed at selected sites in the major climate zones. The BSRN measurements undergo rigorous quality checks to ensure high accuracy as well as homogeneity in the data (Wild et al. 2005). Aerosols have a vital impact on the Earth–atmosphere system through their direct and indirect radiative forcing (e.g., Xia et al. 2007; Zhao and Garrett 2015; Yang et al. 2016b). Several large ground-based sunphotometer networks—for example, the Aerosol Robotic Network (AERONET) (Holben et al. 1998), Photométrie pour le Traitement Opérationnel de Normalisation Satellitaire (PHOTONS) (Goloub et al.

CONTACT ZHANG Jinqiang zjq@mail.iap.ac.cn

2008), and the China Aerosol Remote Sensing Network (CARSNET) (Che et al. 2009)—have been established to characterize the aerosol optical properties that are widely used to validate satellite and model aerosol products.

The BSRN and AERONET-like surface observational networks, which are very applicable for the detailed analysis of regional radiation and aerosols characteristics due to their continuous measurements, have been extensively established in the Beijing–Tianjin–Hebei megacity on the North China Plain (NCP). However, much less attention has been paid to other provinces, such as Shanxi, which is one of the most important coal resources and industrial chemical centers of China and experiences heavy industry pollution. To further our understanding of aerosol properties and their potential effects on the surface energy radiation, an Atmosphere–Aerosol–Cloud–CCN observational campaign was performed at Xinzhou, Shanxi, in summer 2014 (Zhang et al. 2016; Wang et al. 2016; Li et al. 2019). Based on the ground measurements from the campaign, this study analyzed the properties of radiation and aerosol together at this suburban site. The paper is organized as follows: section 2 briefly describes the site and measurements, the main results are presented in section 3, and a conclusion is given in section 4.

2. Site and measurements

2.1 Site

As shown in Figure 1, Xinzhou (38.07°N, 112.12°E; 700 m above sea level), which is ~450 km southwest of Beijing, is located in the middle of Shanxi Province on the NCP. Xinzhou is situated in the temperate continental monsoon climate zone; its annual average temperature and precipitation ranges are 4.3°C–9.2°C and 345–588 mm, respectively.

2.2 Radiation measurement

Comprehensive radiative parameters, including surface global radiation (shortwave radiation: SW), longwave radiation (LW), direct radiation, diffuse radiation, photosynthetically active radiation (PAR), and ultraviolet-A (UVA) and ultraviolet-B (UVB) radiation, were observed with six state-of-the-art Kipp & Zonen radiometers at Xinzhou from 26 June to 13 September 2014. The main specifications of each radiometer are presented in Table 1. The observational data, quality-checked by using the BSRN quality control procedure (Ohmura et al. 1998; Long and Ackerman 2000), were analyzed in this study.

2.3 Aerosol measurement

A Cimel sunphotometer, the standard instrument of AERONET, was deployed at Xinzhou to provide continuous aerosol measurements from 26 June to 13 September 2014. The Cimel measures solar direct spectral radiation at 10 wavelengths from 340 to 1020 nm and sky radiance at four wavelengths (440, 675, 870, and 1020 nm). The uncertainty of aerosol optical depth (AOD) from the direct sun algorithm was 0.01 to 0.02 (Eck et al. 1999). The aerosol inversion algorithm developed by Dubovik and King (2000) was used to derive aerosol physical and optical properties such as the aerosol size distribution, single scattering albedo (SSA), extinction Ångström exponent (EAE), and absorption Ångström exponent (AAE). EAE, a measure of the wavelength dependence of the AOD, is inversely

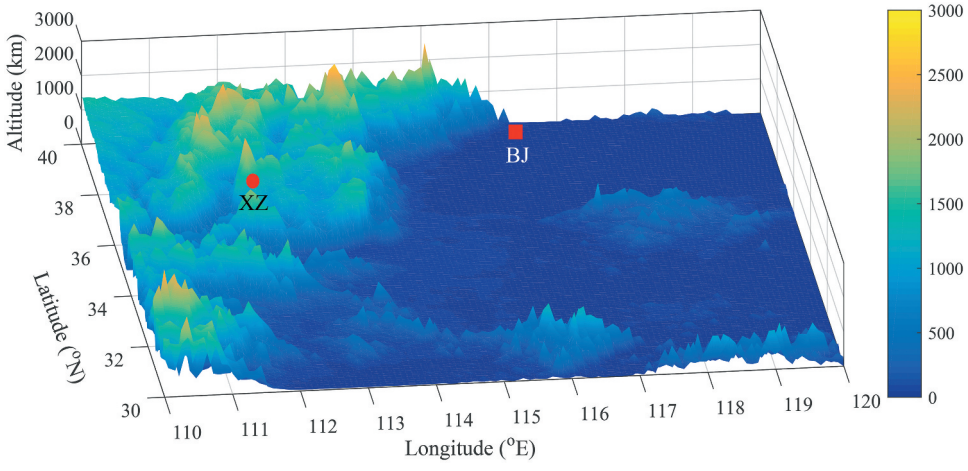

Figure 1. Location of Xinzhou (red dot), ~450 km southwest of Beijing (BJ; red rectangle). The color bar represents the altitude, which is 700 m at Xinzhou.

Table 1. Main specifications of the six radiometers deployed at Xinzhou.

	SW	LW	Direct	Diffuse	PAR	UVA/UVB
Spectral range (μm)	0.2–3.6	4.5–42	0.2–4	0.2–3.6	0.4–0.7	0.315–0.4/0.28–0.315
Response time	< 5 s	< 18 s	< 5 s	< 5 s	< 1 μs	< 1.5 s
Nonlinearity	< 0.2%	< 1%	<0.2%	< 0.2%	< 1%	< 1%

related to the particle size. AAE is a measure of the wavelength dependence of absorptive AOD. The optical parameters of AOD (at 440 nm), SSA (at 440 nm), EAE (440–870 nm), and AAE (440–870 nm) (hereafter simply referred to as AOD, SSA, EAE, and AAE), as well as the size distribution, were analyzed to exhibit the aerosol properties in this study. Additionally, the inversion algorithm–retrieved instantaneous surface solar radiation, aerosol radiative forcing (ARF), and ARF efficiency (ARFE) at the bottom of the atmosphere (BOA) were also used to explore the aerosol direct radiative effect.

3. Results

3.1 Radiation properties

Figure 2 shows the diurnal evolutions of the seven radiation parameters observed under clear and cloudy skies during the study period. The LW was analyzed during a whole 24-h day, and the other six solar radiation parameters were analyzed during the daytime (0600–2000 local standard time (LST)). For the LW variations (Figure 2 (b)), a sigmate structure was presented by a maximum of 392.6 W m^{-2} at 1700 LST associated with the cloud radiative forcing, and a minimum of 360.0 W m^{-2} at 0600 LST when the lowest surface temperature (17.1°C) occurred. The remaining six radiation measurements exhibited a consistent pattern with a single peak at ~1300 LST when the radiation values were 689.9, 352.0, 339.8, 293.6, 11.5, and 1.4 W m^{-2} for SW, direct, diffuse, PAR, UVA, and UVB, respectively (Table 2). Compared to the other parameters, less attention has been paid by the atmospheric science community to PAR, which is one of the critical influencing factors in ecological and agricultural development. Due to the scarcity of observations from regular weather stations, PAR estimations are usually conducted based on the classical climatological method, which considers that PAR is a portion of SW radiation. This consideration results in the proposal of the PAR efficiency factor (PARF), i.e., the proportion of the PAR to the total solar radiation. However, PARF, which is subject to pressure, altitude, clouds, and other factors, is highly variable on both temporal and spatial scales, leading to the proposal of various PARFs from ~0.4 to ~0.6 (e.g., Moon 1940; McCree 1966) that require local calibration. It showed that the diurnal PARF at Xinzhou was generally 0.42, but it was 0.47 at twilight (0600 and 2000 LST).

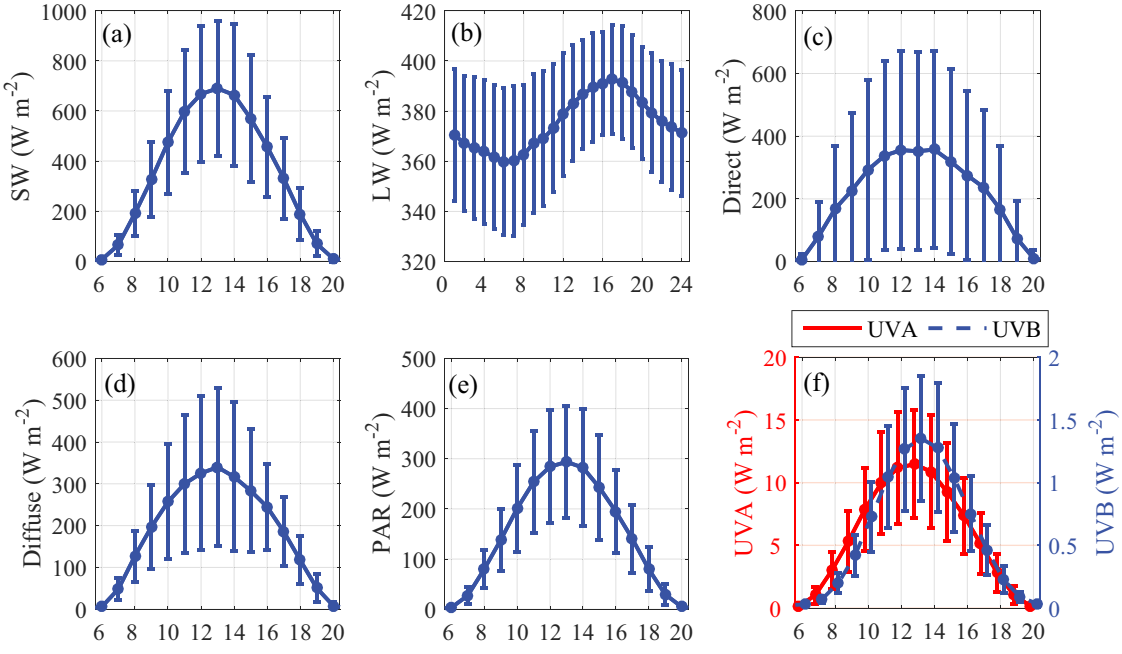

Figure 2. Diurnal evolutions and their standard deviations for different radiation types: (a) SW; (b) LW; (c) direct; (d) diffuse; (e) PAR; and (f) UVA and UVB.

Table 2. Summary of the daily maximum and the daily average over four months for the seven radiation parameters.

	SW	LW	Direct	Diffuse	PAR	UVA	UVB
Daily maximum (W m^{-2})	689.9	392.6	352.0	339.8	293.6	11.5	1.4
Daily averages (W m^{-2})	353.5	375.2	216.9	186.8	150.1	5.8	0.6

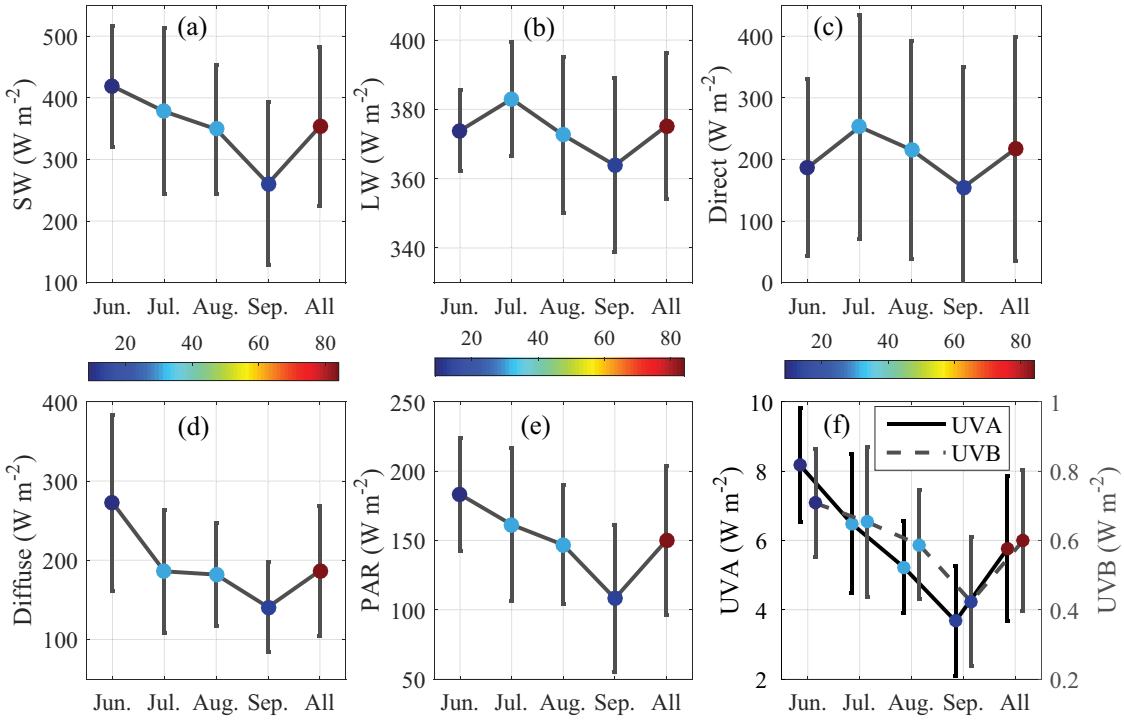

Figure 3. Monthly variations and their standard deviations for different radiation types: (a) SW; (b) LW; (c) direct; (d) diffuse; (e) PAR; and (f) UVA and UVB. The average of each parameter during all months is also shown. The color bar in each panel represents the number of observation days.

Monthly radiation variations between June and September are shown in Figure 3. A uniform decrease is shown by the SW, diffuse radiation, PAR, and UVA and UVB radiation. Except for the relatively small magnitude in June when observational days were limited to some extent, both LW and direct radiation presented a similar monthly decreasing pattern as the above five parameters. The daily average radiation during all four months was 353.5, 375.2, 216.9, 186.8, 150.1, 5.8, and 0.6 W m^{-2} for SW, LW, direct radiation, diffuse radiation, PAR, and UVA and UVB radiation, respectively (Table 2); the monthly mean PARF was 0.43.

3.2 Aerosol properties

The occurrence frequency of AOD derived from the direct sun algorithm is shown in Figure 4(a). There were two intensive areas, i.e., AOD < 0.5 and between 1 and 1.5, accounting for 62.4% and 15.3% of all samples, respectively. The size distribution was bimodal for all AOD measurements, i.e., the accumulation of fine mode aerosols had a peak between 0.1 and 0.2 μm, and that of coarse mode aerosols had a peak at approximately 5 μm (Figure 4(b)). The volume concentrations of fine particles clearly increased with increasing AOD, which was not seen in the coarse particles. Hygroscopic growth of fine particles could be one of potential causes for the increase of fine mode radius (Zhao et al. 2018), which contributes to the increase of aerosol scattering and thereby AOD. Coarse particles in this region are likely related to local emissions by agricultural activities and road transportation.

It was suggested that the high AOD (> 0.4 at 400 nm) leads to robust AERONET retrievals since the sensitivity to retrievals of aerosol optical properties using AERONET direct sun and almucantar sky measurements increases as AOD increases (Dubovik et al. 2000). To ensure reliability of inversion products, only AOD > 0.4 at 440 nm are analyzed hereafter, indicating the domination of coarse mode particles. The instantaneous values of EAE and AAE are shown in Figure 4(c). The EAE, calculated from a linear regression of AOD at 440 and 870 nm versus wavelength at the logarithmic scale, is a parameter

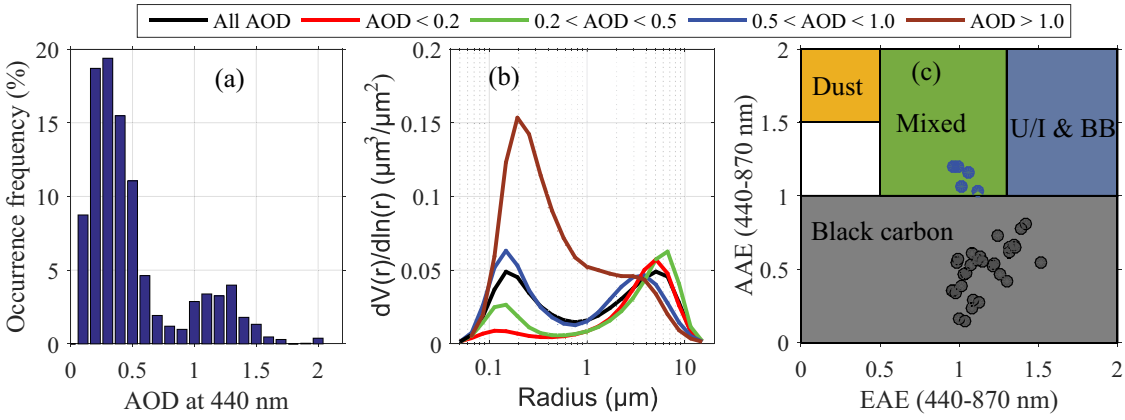

Figure 4. (a) Occurrence frequency of AOD at 440 nm derived from the direct sun algorithm. (b) Aerosol volume size distributions for all AOD (black line) and sorted by different AOD bins, i.e., < 0.2 (red line), 0.2–0.5 (green line), 0.5–1.0 (blue line), and >1.0 (brown line). (c) Distributions of AAE as a function of EAE for the aerosol cases with AOD > 0.4 at 440 nm; the areas with different colors mark the extent of different aerosol types.

reflecting the volume fraction of fine mode aerosols. The AAE, calculated similarly to EAE but using absorptive AOD at these two wavelengths, is an intrinsic property closely related to aerosol chemical components (Giles et al. 2012). Both EAE and AAE were generally less than 1.5; their mean values were 1.14 ± 0.15 and 0.58 ± 0.28, respectively. Previous studies have suggested that the relationship between aerosol absorption and size information is a good indicator for categorizing the dominant aerosol type or optical mixture (Giles et al. 2012). The relationship between EAE and AAE is thus used to classify different aerosol types. The threshold values used here are obtained from previous literature (Giles et al. 2011, 2012; Zhu et al. 2014), specified as follows: (1) the 'dust' category is characterized by EAE < 0.5 and AAE > 1.5; (2) the 'mixed' aerosol type is characterized by 0.5 < EAE < 1.3 and 1.0 < AAE < 2.0; (3) U/I & BB (urban/industrial and biomass-burning) aerosols are divided into a whole category by EAE > 1.3 and 1.0 < AAE < 2.0; and (4) AAE < 1.0 is associated with black carbon coating on coarse particles such as dust and organic carbon (Dubovik et al. 2000; Eck et al. 2010; Giles et al. 2012). Most aerosols at Xinzhou were black carbon coating on coarse particles, accounting for 85.7% of all cases, followed by the mixed aerosol type (14.3%); neither dust nor U/I & BB was observed during our study period. Mixed aerosols have been most frequently reported at AERONET stations on the NCP, such as Xionglong, Xianghe, and Beijing (Giles et al. 2012; Zhu et al. 2014). However, different dominant aerosol types were observed in this study. This is likely because Xinzhou is located in the middle of Shanxi Province, an important energy and industrial chemical center of China (Li et al. 2015, 2017) and an important source of coal combustion emissions in central China (Wang et al. 2016). The characteristics of the site may also lead to the relatively low values of AAE.

3.3 Aerosol radiative effect

Figure 5(a) shows the scatterplots of surface SW calculated by the inversion algorithm as a function of that observed

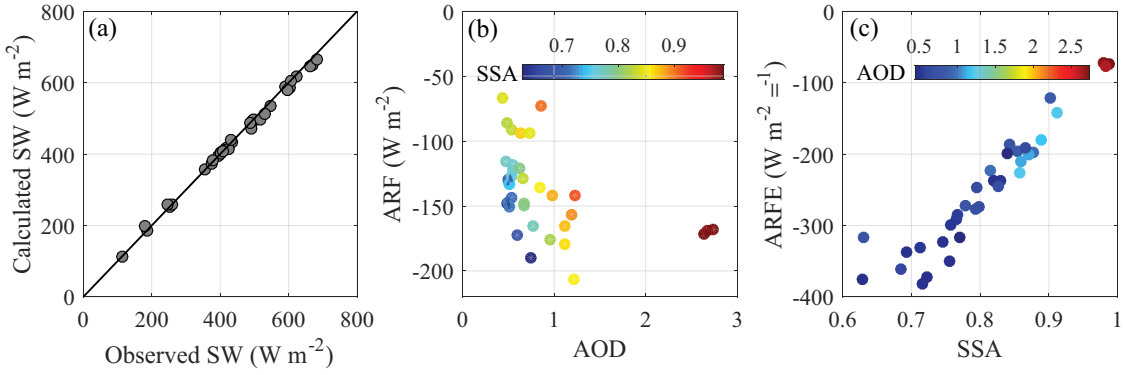

Figure 5. (a) The inversion algorithm–calculated SW as a function of the observed SW. The black line denotes the 1:1 line. (b) Scatterplot of instantaneous ARF at the BOA as a function of AOD and (c) ARFE as a function of SSA derived from the aerosol inversion algorithm. The color bar in panels (b, c) presents the values of SSA and AOD for the data points, respectively.

by the ground radiometer. Overall, the retrievals of observation and calculation agreed well, as shown by all data points falling along or overlapping the 1:1 line. The correlation coefficient, mean bias, and standard deviation between the observations and the calculations were 0.999, 4.02 W m^{-2}, and 9.52 W m^{-2}, respectively. The reasonable performance of the inversion algorithm encourages us to explore the aerosol radiative effect (Figure 5(b)). A negative or positive sign of the ARF determines whether the aerosols produce a cooling or a heating effect. More negative values indicate a stronger cooling effect. The instantaneous ARF at the BOA was generally distributed between −50 and −200 W m^{-2}, with a mean magnitude of −138.9 ± 33.0 W m^{-2}. A gross pattern that the cooling effect of ARF increased with increasing AOD was presented. The ARFE, defined as ARF divided by AOD, was also calculated at Xinzhou. Most ARFE values varied between −100 and −400 W m^{-2}; the average value was −246.4 ± 86.1 W m^{-2} for all cases (Figure 5(c)). It was clearly demonstrated that the cooling effect of ARFE increased with decreasing SSA, which was scattered between 0.6 and 1, with a mean value of 0.81 ± 0.09. The SSA at Xinzhou tended to be lower than the typical values (~0.90) observed at the AERONET stations on the NCP, such as Beijing, Xianghe, and Xinlong (Xia et al. 2006; Li et al. 2007; Zhu et al. 2014). These lower SSA values should be associated with the dominant aerosol type at Xinzhou, i.e., black carbon coating on coarse particles.

4. Conclusions and discussion

This study analyzed the features of summer radiation and aerosol at a suburban site on the NCP. The main conclusions are summarized as follows:

The radiative parameters of SW, diffuse radiation, PAR, and UVA and UVB radiation generally presented a decreasing trend between June and September in 2014 at Xinzhou. The proportion of the PAR to the total solar radiation was 0.43. The mean values of EAE and AAE were 1.14 ± 0.15 and 0.58 ± 0.28 for the aerosol cases with AOD > 0.4 at 440 nm, respectively. Black carbon coating on coarse particles was the most frequent aerosol type (85.7%), which was different from the dominant mixed aerosols at the other AERONET stations on the NCP. This difference led to a lower SSA (0.81) at Xinzhou than the typical values (~0.90) on the NCP. Mean ARF was −138.9 ± 33.0 W m^{-2} at Xinzhou. To ensure reliability of aerosol products, only aerosol cases with AOD > 0.4 are analyzed, indicating that the ARF was somewhat overestimated than that by the consideration of fine mode particles. It should also be noted that the representativeness of the results in this study still needs further verification given they are obtained from relatively short-term measurements at a single point. More long-term field studies would help us further enhance our knowledge of aerosol properties and its radiative impacts on the NCP.

Disclosure statement

No potential conflict of interest was reported by the authors.

Funding

This work was supported by the National Key R&D Program of China [grant number 2017YFA0603504] and the National Natural Science Foundation of China [grant number 41875183].

References

Anderson, T. L., R. J. Charlson, S. E. Schwartz, R. Knutti, O. Boucher, H. Rodhe, and J. Heintzenberg. 2003. "Climate Forcing by Aerosols—A Hazy Picture." *Science* 300: 1103–1104. doi:10.1126/science.1084777.

Che, H., X. Zhang, H. Chen, B. Damiri, P. Goloub, Z. Li, X. Zhang, et al. 2009. "Instrument Calibration and Aerosol Optical Depth Validation of the China Aerosol Remote Sensing Network." *Journal of Geophysical Research* 114: D03206. doi:10.1029/2008jd011030.

Dubovik, O., and M. D. King. 2000. "A Flexible Inversion Algorithm for Retrieval of Aerosol Optical Properties from Sun and Sky Radiance Measurements." *Journal of Geophysical Research* 105: 20673–20696. doi:10.1029/2000JD900282.

Dubovik, O., A. Smirnov, B. N. Holben, M. D. King, Y. J. Kaufman, T. F. Eck, and I. Slutsker. 2000. "Accuracy Assessments of Aerosol Optical Properties Retrieved from AERONET Sun and Sky-radiance Measurements." *Journal of Geophysical Research* 105: 9791–9806. doi:10.1029/2000JD900040.

Eck, T. F., B. N. Holben, J. S. Reid, O. Dubovik, A. Smirnov, N. T. O'Neill, I. Kinne, and S. Slutsker. 1999. "Wavelength Dependence of the Optical Depth of Biomass Burning, Urban, and Desert Dust Aerosols." *Journal of Geophysical Research* 104: 31333–31349. doi:10.1029/1999JD900923.

Eck, T. F., B. N. Holben, A. Sinyuk, R. T. Pinker, P. Goloub, H. Chen, B. Chatenet, et al. 2010. "Climatological Aspects of the Optical Properties of Fine/coarse Mode Aerosol Mixtures." *Journal of Geophysical Research* 115: D19. doi:10.1029/2010jd014002.

Fan, H., C. Zhao, and Y. Yang. 2020. "A Comprehensive Analysis of the Spatio-temporal Variation of Urban Air Pollution in China during 2014–2018." *Atmospheric Environment* 220: 117066. doi:10.1016/j.atmosenv.2019.117066.

Garrett, T., and C. Zhao. 2006. "Increased Arctic Cloud Longwave Emissivity Associated with Pollution from Mid-latitudes." *Nature* 440: 787–789. doi:10.1038/nature04636.

Giles, D. M., B. N. Holben, T. F. Eck, A. Sinyuk, A. Smirnov, I. Slutsker, R. R. Dickerson, et al. 2012. "An Analysis of AERONET Aerosol Absorption Properties and Classifications Representative of Aerosol Source Regions." *Journal of Geophysical Research* 117: D17. doi:10.1029/2012JD018127.

Giles, D. M., B. N. Holben, S. N. Tripathi, T. F. Eck, W. W. Newcomb, I. Slutsker, R. R. Dickerson, et al. 2011. "Aerosol Properties over the Indo-Gangetic Plain: A Mesoscale Perspective from the

TIGERZ Experiment." *Journal of Geophysical Research* 116: D18. doi:10.1029/2011jd015809.

Goloub, P., Z. Li, O. Dubovik, L. Blarel, T. Podvin, I. Jankowiak, R. Lecoq, et al. 2008. "PHOTONS/AERONET Sunphotometer Network Overview: Description, Activities, Results." *Proceedings of SPIE* 6936: 1. doi:10.1117/12.783171.

Holben, B. N., T. F. Eck, I. Slutsker, D. Tanre, J. P. Buis, A. Setzer, E. Vermote, et al. 1998. "AERONET—A Federated Instrument Network and Data Archive for Aerosol Characterization." *Remote Sensing of Environment* 66: 1–16. doi:10.1016/S0034-4257(98)00031-5.

Li, J., P. Li, L. Yuan, Y. Yin, Z. Wang, J. Li, Y. Li, et al. 2017. "Physical and Optical Properties of Atmospheric Aerosols in Summer at a Suburban Site in North China." *Aerosol and Air Quality Research* 17: 1474–1488. doi:10.4209/aaqr.2016.12.0525.

Li, J., Y. Yin, P. Li, Z. Li, R. Li, M. Cribb, Z. Dong, et al. 2015. "Aircraft Measurements of the Vertical Distribution and Activation Property of Aerosol Particles over the Loess Plateau in China." *Atmospheric Research* 155: 73–86. doi:10.1016/j.atmosres.2014.12.004.

Li, Z., H. Chen, M. Cribb, R. Dickerson, B. Holben, C. Li, D. Lu, et al. 2007. "Preface to Special Section on East Asian Studies of Tropospheric Aerosols: An International Regional Experiment (EAST-AIRE)." *Journal of Geophysical Research* 112: D22S00. doi:10.1029/2007JD008853.

Li, Z., Y. Wang, J. Guo, C. Zhao, M. Cribb, X. Dong, J. Fan, et al. 2019. "East Asian Study of Tropospheric Aerosols and Their Impact on Regional Clouds, Precipitation, and Climate (EAST-AIR$_{CPC}$)." *Journal of Geophysical Research* 124: 13026–13054. doi:10.1029/2019JD030758.

Long, C. N., and T. P. Ackerman. 2000. "Identification of Clear Skies from Broadband Pyranometer Measurements and Calculation of Downwelling Shortwave Cloud Effects." *Journal of Geophysical Research* 105: 15609–15626. doi:10.1029/2000JD900077.

McCree, K. J. 1966. "A Solarimeter for Measuring Photosynthetically Active Radiation." *Agricultural Meteorology* 3: 353–366. doi:10.1016/0002-1571(66)90017-3.

Moon, P. 1940. "Proposed Standard Solar-radiation Curves for Engineering Use." *Journal of the Franklin Institute* 230: 583–617. doi:10.1016/S0016-0032(40)90364-7.

Ohmura, A., E. G. Dutton, B. Forgan, C. Fröhlich, H. Gilgen, H. Hegner, A. Heimo, et al. 1998. "Baseline Surface Radiation Network (BSRN/WCRP): New Precision Radiometry for Climate Research." *Bulletin of the American Meteorological Society* 79: 2115–2136. doi:10.1175/1520-0477(1998)079<2115:bsrnbw>2.0.co;2.

Pounds, J. 2001. "Climate and Amphibian Declines." *Nature* 410: 639–640. doi:10.1038/35070683.

Wang, Q., J. Zhao, W. Du, G. Ana, Z. Wang, L. Sun, Y. Wang, et al. 2016. "Characterization of Submicron Aerosols at a Suburban Site in Central China." *Atmospheric Environment* 131: 115–123. doi:10.1016/j.atmosenv.2016.01.054.

Wild, M., H. Gilgen, A. Roesch, A. Ohmura, C. N. Long, E. G. Dutton, B. Forgan, et al. 2005. "From Dimming to Brightening: Decadal Changes in Solar Radiation at Earth's Surface." *Science* 308: 847–850. doi:10.1126/science.1103215.

Xia, X., H. Chen, P. Wang, W. Zhang, P. Goloub, B. Chatenet, T. F. Eck, et al. 2006. "Variation of Column-integrated Aerosol Properties in a Chinese Urban Region." *Journal of Geophysical Research* 111: D05204. doi:10.1029/2005JD006203.

Xia, X., Z. Li, P. Wang, H. Chen, and M. Cribb. 2007. "Estimation of Aerosol Effects on Surface Irradiance Based on Measurements and Radiative Transfer Model Simulations in Northern China." *Journal of Geophysical Research* 112: D22. doi:10.1029/2006JD008337.

Yang, X., C. Zhao, J. Guo, and Y. Wang. 2016b. "Intensification of Aerosol Pollution Associated with Its Feedback with Surface Solar Radiation and Winds in Beijing." *Journal of Geophysical Research* 121: 4093–4099. doi:10.1002/2015JD024645.

Yang, X., C. Zhao, L. Zhou, Y. Wang, and X. Liu. 2016a. "Distinct Impact of Different Types of Aerosols on Surface Solar Radiation in China." *Journal of Geophysical Research* 121: 459–6471. doi:10.1002/2016JD024938.

Zhang, F., Z. Li, Y. Li, Y. Sun, Z. Wang, P. Li, L. Sun, et al. 2016. "Impacts of Organic Aerosols and Its Oxidation Level on CCN Activity from Measurements at a Suburban Site in China." *Atmospheric Chemistry and Physics* 16: 5413–5425. doi:10.5194/acp-16-5413-2016.

Zhao, C., and T. J. Garrett. 2015. "Effects of Arctic Haze on Surface Cloud Radiative Forcing." *Geophysical Research Letters* 42: 557–564. doi:10.1002/2014GL062015.

Zhao, C., Y. Li, F. Zhang, Y. Sun, and P. Wang. 2018. "Growth Rates of Fine Aerosol Particles at a Site near Beijing in June 2013." *Advances in Atmospheric Sciences* 35: 209–217. doi:10.1007/s00376-017-7069-3.

Zhu, J., H. Che, X. Xia, H. Chen, P. Goloub, and W. Zhang. 2014. "Column-integrated Aerosol Optical and Physical Properties at a Regional Background Atmosphere in North China Plain." *Atmospheric Environment* 84: 54–64. doi:10.1016/j.atmosenv.2013.11.019.